NASA
Technical
Paper
2538

March 1986

Testing of YUH-61A Helicopter Transmission in NASA Lewis 2240-kW (3000-hp) Facility

Andrew M. Mitchell,
Fred B. Oswald, and
Fredrick T. Schuller

NASA

NASA
Technical
Paper
2538

1986

Testing of YUH-61A Helicopter Transmission in NASA Lewis 2240-kW (3000-hp) Facility

Andrew M. Mitchell,
Fred B. Oswald, and
Fredrick T. Schuller

Lewis Research Center
Cleveland, Ohio

National Aeronautics
and Space Administration

**Scientific and Technical
Information Branch**

Summary

A helicopter transmission that was being considered for the Army's Utility Tactical Transport Attack System (UTTAS) was tested in the NASA Lewis 2240-kW (3000-hp) test facility to obtain the transmission's operational data. The results will form a vibration and efficiency data base for evaluating similar-class helicopter transmissions. The transmission's mechanical efficiency was determined to be 98.7 percent at its rated power level of 2080 kW (2792 hp). At power levels up to 113 percent of rated the transmission displayed 56 percent higher vibration acceleration levels on the right input than on the left input. Both vibration signature analysis and final visual inspection indicated that the right input spiral-bevel gear had poor contact patterns.

The highest vibration meter level was 52 g's rms at the aft accessory gear, which had free-wheeling gearsets (the transmission was tested without accessories). At 113-percent power and 100-percent rated speed the vibration meter levels generally ranged from 3 to 25 g's rms. The facility was operated at and qualified for testing to 2600 kW (3500 hp).

Introduction

Modern helicopter transmissions are being required to achieve ever-higher levels of mechanical efficiency and transmitted power per unit weight (P/W) and significantly longer mean times between unscheduled removals (MTBUR). A transmission's mechanical efficiency is to a large degree an index of its design sophistication. A 2240-kW (3000-hp) helicopter transmission is nearly 98 percent efficient at full rated load. Each of the many items in a helicopter gear train—gears, bearings, lubrication system circuitry, and seals—influences the total efficiency. In general there is a 3/4-percent loss for a planetary gear stage and a 1/2-percent loss for a single bevel or spur gear mesh (ref. 1). Further data on gear and gear system power losses can be found in references 2 to 5. The effect of lubrication and oil at gear meshes is reported in references 6 to 8. Oil traction effects on worm gear efficiencies are covered in reference 9. Bearing power losses are reviewed in reference 10. Even small efficiency degradations (e.g., an accumulative reduction of nearly 1 percent) are very significant (ref. 11). Efficiency studies on the Army's smaller OH–58 helicopter transmission have also shown that even the composition of oils obtained under the same military specification has a significant effect (refs. 12 and 13).

A limitation to designing lighter weight geared transmissions arises from the dynamic tooth loads and noise produced by vibration within the transmission. Gearbox vibration is caused primarily by tooth meshing excitation and is characterized by a discrete rather than a continuous line spectrum. Excessive vibration may result if any of the meshing frequencies or strong sidebands happen to nearly coincide with a natural vibration frequency resonance of the transmission. In highly loaded, lightweight, fatigue-critical gearing such as that in helicopter transmissions, resonance is a much more critical phenomenon than in heavy-duty industrial drives (ref. 14). Further descriptions of the vibratory response of gearing are given in references 15 to 19.

For many years the two major conflicting field-operational performance indices, MTBUR (ref. 20) and P/W (ref. 21), have remained in need of substantial improvement. Field experience has shown that lighter, more flexible transmissions (for the same power) tend to be noisier. Because of the complexity of helicopter transmissions and the effect of component "coupling" on design, improvements in these indices require continuing programs of advanced analytical research and testing of the life, efficiency, and noise of full-scale transmissions. These programs will validate advanced components and technologies against the research and computer codes that spawned them. The NASA Lewis facility augments the ongoing need for facilities that can quantitatively evaluate technological research concepts in order to improve the conflicting requirements of increasing both MTBUR and P/W. The facility will help to advance helicopter transmission technology (refs. 22 to 24).

This work was conducted primarily to develop baseline efficiency and vibration data for the YUH–61A transmission to serve as documentation for improvements to transmission designs. A secondary objective was to establish the operational and control limits and integrity of the test facility. The data acquisition system is overviewed as well as the facility and its subsystems. Test results include transmission power ranges, mechanical efficiency, and vibration characteristics.

Apparatus

Test Transmission

The YUH–61A helicopter transmission was a candidate in the U.S. Army's Utility Tactical Transport Attack System (UTTAS) competition. It has a rated power level of 2080 kW

(2792 hp) and an output rotor shaft speed of 286 rpm. The transmission (figs. 1 to 3) delivers power from the UTTAS helicopter's twin engines through separate external speed-reduction stages and twin input spiral-bevel gears to a combining spiral-bevel gear. This combining gear in turn is splined to the sun gear of a single-planetary-gear output stage. The input spiral-bevel gears provide a reduction of 121/25 from the input shaft speed of 7178 rpm. The planetary stage provides a further reduction ratio of 1+113/27. The overall speed reduction is 25.096. The numbers of gear teeth, the shaft speeds, and the calculated tooth meshing frequencies and their harmonics are listed in table I. The transmission was tested without its forward accessory gearbox. The aft accessory gearbox was mounted without the auxiliary power unit or generator installed. The main transmission has a dry weight of 383.3 kg (845 lb), the housing being primarily of magnesium with an aluminum upper cover. The lubricant for this transmission complied with the MIL–L–7808 specification.

The transmission's integral lubrication system (ref. 25) consists of a primary system and an auxiliary system. The primary lubrication pump has two elements: a pressure element and a scavenge element. The auxiliary lubrication pump is a single-element pump driven by the forward accessory spiral-bevel gear.

Test Facility

The NASA Lewis 2240-kW (3000-hp) helicopter transmission facility is a regenerative (four square) testing power

TABLE I.—SHAFT SPEEDS AND TOOTH MESHING HARMONICS FOR RATED OPERATING SPEED OF 286 rpm

Component	Number of teeth	Shaft speed, rpm	First mode	Second mode	Third mode	Fourth mode	First mode	Second mode	Third mode	Fourth mode
			Shaft harmonics, Hz				Tooth harmonics, Hz			
Main power train										
Input bevel pinion	25	7 178	119.6	239	359	479	2991	5981	8 972	11 963
Main bevel gear	121	1 483	24.72	49.4	74.1	98.9	2991	5981	8 972	11 963
Main-bevel sun gear	27	1 483	[a]24.72	49.4	74.1	98.9	539	1077	1 616	2 155
Planet gears (four)	43	466	[a]7.76	15.5	23.3	31.0	539	1077	1 616	2 155
Ring gear	113	0	(a)	-----	----	-----	539	1077	1 616	2 155
Carrier (output)	----	286	4.77	9.53	14.3	19.1	----	-----	-----	-----
Planet passing frequency	----	-----	19.07	38.1	57.2	76.3	----	-----	-----	-----
Tail rotor										
Main bevel gear	121	1 483	24.72	49.4	74.1	98.9	2991	5981	8 972	11 963
Tail takeoff gear	25	7 178	119.6	239	359	479	2991	5981	8 972	11 963
Shell gear	28	7 178	119.6	239	359	479	3350	6699	10 049	13 398
Tail drive gear	30	6 699	111.7	223	335	447	3350	6699	10 049	13 398
Rear accessory gearbox										
Accessory drive	42	6 999	116.7	223	335	447	4689	9379	14 068	18 757
Spur gear to clutch	49	5 742	95.70	191	287	383	4689	9379	14 068	18 375
Spur gear from clutch	48	5 742	95.70	191	287	383	4594	9187	13 781	
Primary lubrication pump	49	5 625	93.75	187	281	375				
Idler gear	55	5 011	83.52	167	251	334				
Fan gear	33	8 352	139.2	278	417	557				
Primary lubrication pump	49	5 625	93.75	187	281	375				
Hydraulic pump	36	7 656	127.6	255	383	510				
Lubricant scavenge pump	48	5 742	95.70	191	287	383				
Idler gear	60	4 594	76.56	153	230	306				
Generator drive	23	11 983	199.7	399	599	799				
Idler gear	60	4 594	76.56	153	230	306				
Auxiliary-power-unit gear	36	7 656	127.6	255	383	510				

[a]Shaft frequencies for sidebands (relative to carrier: sun gear, reduced to 19.95 Hz; planet gears, increased to 12.53 Hz; ring gear, 4.77 Hz).

loop driven by a constant-speed, 600-kW (800-hp) induction motor. The test stand was designed and built by the Boeing-Vertol Company. Speed control is provided by a dynamic (eddy current) clutch (fig. 4). The induction motor drive serves only to supply the mechanical frictional losses in the power loops. A 90° reduction gearbox connects the clutch to an input helical pinion gear located in the power distribution gearbox (fig. 5). The pinion gear in turn drives the large helical combining gear connected to the rotor output shaft and the smaller helical pinion gear on the opposite side. Torque is introduced into both rotating vertical shafts (representing the left and right transmission drive engines) by two two-stage planetary torquers. The upper ring gears of these torquers have external teeth that mesh with dc-motor-driven worm gears. Upon ring gear rotation a controlled torque is introduced into the rotating left and right shafts. Power flows through the input stage of the facility gearbox, through the transmission, and out the rotor shaft and is recirculated through the power distribution gearbox. The returning power flow to the two pinions completes the power flow loop. The transmission tail output shaft and torquer loop are similar (recirculating), but the controlled power flow is reversed to simulate the power requirements of the UTTAS helicopter's tail rotor.

Immediately above the transmission and connected to its output rotor shaft is the rotor loader assembly. The loader assembly housing is attached to three vertical hydraulic cylinders positioned above it and located at three position points that fall on the apexes of an equilateral triangle. A fourth cylinder is attached and reacts horizontally. Controlling the cylinder pressures produces a bending moment in the transmission's output shaft to simulate flight lift, two-axis moment, and drag (horizontal) loading. During operational testing the input speeds, torques, and rotor loads are controlled from a remote control room.

The lubrication system of the facility consists of two pumps rated at 0.66 m^3/min (173 gal/min) and 690 kPa (100 psi) with oil flowing through three tube-and-shell oil/water heat exchangers located above the sump. The heat exchangers supply temperature-controlled oil to the facility's gearboxes and torquers. Ten-μm filters are installed in each lubrication output branch. Lubrication oil temperatures and pressures to all facility gearboxes and torquers are connected to limit-warning annunciators. The facility lubrication oil is ASLE grade S-315.

The water system, from the cooling towers, supplies water at 586 kPa (85 psi) for the dynamic clutch and the facility oil/water heat exchangers.

Upon annunciator warning the CO_2 "cell flood" system can be manually activated. Four television cameras allow control room monitoring of the facility during testing. The facility has four flame detector "fire eyes" with fault self-checking circuitry.

The output rotor shaft speed is measured by an inductive speed pickup. Input and tail torques are measured, controlled, and displayed by a telemetry torsion measurement system that uses strain gauge bridges on the rotating shafts. The system was calibrated at torque intervals via the deadweight moment method.

Vibration transducers were commercial piezoelectric accelerometers. All thermocouples were Chromel/Alumel.

The NASA Lewis data acquisition system, Escort II (fig. 6), supports the steady-state experimental facilities at the Lewis Research Center (fig. 6). Escort II has real-time data acquisition and processing capability for up to 256 channels of measurement while maintaining a 2- to 3-sec update rate of facility displays. Mainframe computing capabilities are also available in the off-line batch mode. Data accumulated during testing are analyzed according to computer codes.

Procedure

Efficiency Tests

The test transmission was insulated to provide an adiabatic enclosure. Ten- to 15-cm (4- to 6-in.) thick blankets of fiberglass covered with an aluminized coated asbestos cloth were placed on the top and bottom of the enclosure. The vertical sides of the transmission's sheet metal housing were internally lined with 2.5 cm (1 in.) of fiberglass insulation board and blankets. In addition, a series of 5-cm (2-in.) thick removable fiberglass blankets, similar to the top and bottom blankets, were wrapped around the sides of the transmission (fig. 7). In addition, closed-cell insulation foam was pressure fed into the openings of the enclosure required for the input and tail shafts. A close-fitting stainless steel tube over the transmission shafts (used as an insulation foam stop) permitted the nearly complete adiabatic encapsulation. The transmission had minor heat losses through the annuli of the input and tail shafts and by convection and radiation from the housing. Twelve thermocouples were placed on the sheet metal housing and on top of the upper transmission insulation blankets. One thermocouple was placed in each shaft annulus to allow calculation of all of the heat losses (refs. 26 and 27) from the housing. The flight oil/air heat exchanger (fig. 1), which was close coupled to the transmission, was not enclosed.

The testing comprised varying the output speed and torque under a matrix of set points (table II). Input power levels ranged from 3 to 113 percent of rated power at output rotor speeds of 25, 75, and 100 percent of nominal rated.

For each data point the specified torque and speed were set and the transmission operated at that setting until the close-coupled flight oil/air heat exchanger brought the oil inlet temperature to equilibrium. Data taken included oil inlet and exit temperatures and mass flow rates through the oil/air heat exchanger, the speeds and torques of the input shafts, and the temperatures of the transmission's sheet metal housing. Transmission power loss, input power, and housing heat loss were determined. The mechanical efficiency of the transmission was calculated by

TABLE II.—YUH-61A TR[illegible]
TEST DATA

Escort reading	Speed, percent of rated	Torque, percent of rated	Power, percent of rated
259	25	54	12
260	73	56	41
261	99	57	56
262	27	84	23
263	73	87	64
264	99	86	85
265	27	111	30
266	73	112	82
267	100	113	113
268	27	11	3
269	74	10	7
270	99	11	11
271	99	110	109
272	73	109	80
273	25	109	27
274	100	88	88
275	74	86	64
276	99	57	56
277	25	84	21
278	74	58	43
279	100	11	11
280	27	56	15
281	74	12	9
282	25	12	3
283	26	10	3
284	74	11	8
285	99	11	11
286	99	29	29
287	25	56	14
288	74	57	42
289	99	57	56
290	26	86	22
291	74	87	64
292	98	86	84
293	28	111	31
294	26	112	29
295	73	114	83
296	99	114	113

$$E=\frac{P_i-(P_1+P_2)}{P_i}\times 100$$

where

E mechanical efficiency, percent

P_i transmission input power

P_1 transmission mechanical power loss to heat exchanger

P_2 heat radiation, convection, and conduction power losses through housing and shafts

Vibration Tests

Eleven piezoelectric accelerometers, labeled VIB 1 to VIB 11, were fitted to various locations on the transmission case. Data from eight of the accelerometers (figs. 1 to 3 and table III) are discussed in this report. The frequency response of these eight accelerometers was ±5 percent at 2 to 5500 Hz and +20 percent at 10 kHz. The resonant frequency was 27 kHz.

In the vibration measurement system (fig. 8) the accelerometer output was fed to vibration meters (charge amplifiers) that produced a dc output representing the overall peak acceleration level. The dc signal was converted to digital format for processing by the Escort II system. The vibration meters also produced an ac output signal that was further amplified by broadband amplifiers and stored on 14-channel tape for later analysis on a Fourier analyzer. The vibration measurement system was calibrated by means of signal injection applied at the transmission to check the cabling, the amplifier, and the analyzer system. The calibration was also verified by a shake table.

Data were acquired at several combinations of speed and torque (table II) from less than 5 to 113 percent of full rated power. The tail torque was maintained throughout testing at a nominal 17 percent of the total input torque. Frequency domain vibration spectra were plotted on a Fourier analyzer by using the random (Hanning) signal window. A gearbox produces a discrete spectrum of frequency peaks corresponding to gear meshing harmonics and sidebands above a much lower continuous background of other component noise levels. Because the spectrum is not continuous, the ordinates on the vibration spectral plots are calibrated in units of rms g's and not in $(g's)^2/Hz$ as in a power spectral density plot of a continuous spectrum (ref. 16). Overall (Fourier) acceleration values were obtained for comparison with the vibration meter (Escort II) reading (table III). These were derived by taking the square root of the sum of the squares of the frequency lines in the amplitude spectrum over the measurement bandwidth. Except for "zoom" measurements the frequency range 0 to 12.8 kHz was chosen to provide a frequency resolution of 25 Hz. Twenty data samples were averaged by the analyzer for each vibration spectrum.

Post-Test Inspection

At the conclusion of efficiency and vibration testing of the YUH-61A the transmission was removed from the test stand and disassembled to allow visual inspection at the component level. Oil samples were taken for oil particle analysis. Chip detectors, filters, and the interior housing surfaces of the transmission were also visually inspected. Photographs were taken of the power train gearing components. Gear teeth

TABLE III.—MAJOR FREQUENCY COMPONENTS AT 99 PERCENT OF RATED SPEED AND 113 PERCENT OF RATED TORQUE

Acceler-ometer, VIB-	Accelerometer location	Overall acceleration, g's rms	Component frequency, Hz	Component acceleration, g's rms	Peak-to-peak displacement, μm	
11	Aft accessory drive case	48.5	525	4.2	10.7	Planet mesh
			2975	16.4	1.3	Main bevel
			4650	8.8	.3	Accessory drive
			9325	20.6	.2	Accessory drive
			3325	9.0	.6	Tail drive
			6650	22.2	.4	Tail drive
			9975	12.0	.1	Tail drive
8	Right input	41.7	525	5.4	13.8	Planet mesh
			2975	13.5	1.1	Main bevel
			5925	22.5	.5	Main bevel
7	Forward accessory pinion	35.8	525	3.3	8.4	Planet mesh
			1075	3.5	2.1	Planet mesh
			2975	30.9	2.5	Main bevel
			5925	3.8	.1	Main bevel
9	Left input	24.3	525	8.1	20.6	Planet mesh
			1075	2.8	1.7	Planet mesh
			2975	10.0	.8	Main bevel
			5925	5.8	.1	Main bevel
5	Rotor housing (45°)	16.5	525	1.1	2.8	Planet mesh
			1075	11.5	7.0	Planet mesh
			1600	3.5	1.0	Planet mesh
			2975	5.7	.5	Main bevel
6	Rotor housing (horizontal)	16.4	525	9.8	25.0	Planet mesh
			1075	9.3	5.7	Planet mesh
			1600	2.6	.7	Planet mesh
			2975	1.9	.2	Main bevel
2	Left input (horizontal)	15.6	525	3.2	8.2	Planet mesh
			1075	5.5	3.3	Planet mesh
			1600	2.9	.8	Planet mesh
			2975	9.0	.7	Main bevel
3	Mounting arm	13.0	525	2.2	5.6	Planet mesh
			1075	1.4	.9	Planet mesh
			1600	5.9	1.6	Planet mesh
			2975	2.5	.2	Main bevel

adjacent to any gear tooth contact patterns (footprints) to be observed were whitened so as to highlight the footprints by light reflectance.

Results and Discussion

Efficiency

For the efficiency test 38 data points were taken for a matrix of nominal percentages of rated speed and input torque (table II). The resulting power levels are also shown.

The transmission's mechanical efficiency was 98.7 percent at its rated power level of 2080 kW (2792 hp) and rated output rotor speed of 286 rpm (fig. 9). This was only 0.1 percent higher than the value listed in reference 25. Figures 9 and 10 show the marked effect of speed on efficiency. Past NASA transmission programs (refs. 4, 5, 11, and 13) have shown that the higher efficiencies at 15 to 80 percent of rated load are a direct result of speed-related losses. Lubricant churning, windage, mesh (elastohydrodynamic, rolling traction), and bearing losses all are functions of speed; so operation at lower speed (for a specific input torque) results in reduced net losses

and higher efficiency but at the penalty of operation at less than rated power. Sliding losses also significantly increase nearly in direct proportion to power except at very low torque levels (ref. 4). At torque levels less than 15 percent (fig. 11) the sliding losses approached zero and the power loss approached the tare (no load) loss. As the input power was further reduced, it very rapidly approached the almost constant tare loss, thereby resulting in the very rapid decrease in efficiency. Figure 11 also shows the effect of very low torque operation with increasing speed (at approximately 11 percent of nominal rated torque). The major losses at this loading—churning, windage, mesh, and bearing losses—became significantly more dominant as speed was increased. At full power all losses were contributors, their ratios being dependent on the transmission's design and configuration.

Figures such as 9 to 11 can be useful for comparing the operational integrity of any two similar helicopter transmission designs when used in conjunction with other information such as vibration spectra analyses and wear metal and contamination analyses of the lubricating oil (refs. 28 and 29).

Vibration

Gear vibration is caused by nonuniform action (transmission error) of the gear teeth as they roll through the mesh. Mark (ref. 19) defines mean and random components of transmission error. The mean component, which is the same for all teeth, is due to deviation of the average tooth surface from a perfect involute shape. These deviations are caused by manufacturing errors as well as load-dependent tooth distortion (refs. 19 and 30). The mean component of transmission error produces vibration at the harmonics of the tooth meshing frequency. The random component of transmission error produces vibration at the sideband frequencies. Amplitude modulation (AM) sidebands are excited primarily by eccentricity (runout), which causes the depth of gear tooth engagement to vary as the gears rotate. AM sidebands occur at frequencies equal to the meshing frequency plus or minus multiples of the pinion or gear shaft frequency. Frequency modulation (FM) sidebands are excited by tooth spacing errors or by torsional vibration of the gear shafts (refs. 31 to 34). The combination of AM and FM may produce additional sidebands known as complex intermodulation components (ref. 15).

Any rigid body constrained by elastic supports will have natural modes of vibration at frequencies determined by the effective mass and stiffness properties of the system. A continuous structure will also have an infinite number of flexible body modes (independent of support conditions), each of which has a unique shape and frequency. In practice, however, one need not be concerned with modes of higher frequency than the first two to three harmonics of the highest excitation frequency (ref. 14).

The vibration levels reported by Escort II (converted to g's rms) are plotted in figure 12. (Readings made within ±5 percent of the same speed and torque conditions were averaged.) This figure shows the effect of speed and torque (load) on vibration levels at various points on the transmission. The vibration level generally increased with speed and to a lesser extent with torque.

Vibration spectra from tape-recorded vibration signals for five accelerometers at six speed/torque combinations are shown in figures 13 to 19. These spectra were taken at speeds of 75 and 100 percent of nominal rated with torque levels of 112, 88, and 58 percent and 113, 88, and 11 percent of nominal rated, respectively. A speed map and zoom spectra are provided for VIB 8 (figs. 16 and 17). Spectra for VIB 6 and 7 are shown in figure 20.

The major frequency components at the full-speed, 113-percent-torque operating condition are summarized in table III. An overall acceleration value from the spectral plots (figs. 13 to 15 and 18 to 20) is shown. This value generally agreed within ±6 percent with the vibration meter reading as recorded by the Escort system (converted to rms). The peak-to-peak (double amplitude) displacement at each of the various frequency components is also given in table III.

Very high vibration levels (30 to 50 g's rms) were found at three locations on the test transmission: VIB 11, on the aft accessory gearbox; VIB 8, at the right input pinion; and VIB 7, at the forward accessory pinion. All other accelerometers produced much lower vibration levels.

VIB 11.—The VIB 11 (aft accessory gearbox) vibration meter level (fig. 12(h), 99-percent speed, 113-percent torque) was 51.7 g's. This very high vibration level was due to the several gear meshes (11) located in and near the aft accessory gearbox. The most prominent contributors to the vibration levels were the main bevel, tail drive, and accessory drive meshes (fig. 19). The planet mesh components had a much lower effect. The general trend that larger vibration amplitudes were associated with spiral-bevel gears rather than spur gears in a planetary stage is consistent with prior testing experience involving several transmissions of various sizes (ref. 20). The vibration amplitude at VIB 11 was much more affected by operating speed than by load level. (This was expected since no accessories were mounted and therefore the accessory gears were not loaded.) The spectra taken at 100-percent speed at the various torque levels show much more high-frequency harmonic content than do those taken at 75-percent speed (fig. 19).

VIB 8.—The spectra from VIB 8 at the right input pinion at nominally 100-percent speed (figs. 15(d) to (f)) reveal a band of increased vibration between 4500 and 6000 Hz that contains several prominent response peaks. These peaks were caused by the second harmonic of the main bevel gear meshing (5981 Hz) and by the ninth (4851 Hz) and tenth (5390 Hz) harmonics of the planet gear meshing. These tooth meshing harmonics were excited by the mean component of transmission error. When the operating speed was reduced from the 100-percent (286 rpm) level, these peaks were shifted out of the 4500- to 6000-Hz band (figs. 15(a) to (c)) and greatly reduced in amplitude, but the background vibration level within this band remained higher than outside the band. The band

of increased vibration suggests resonant response. A speed map of VIB 8 (fig. 16) was made at the 11-percent torque condition. The speed map shows a very strong component at the main bevel gear meshing frequency (2991 Hz) as 100-percent speed was reached and a tendency toward many minor vibration peaks within the 4500- to 6000-Hz band at speeds approaching 100 percent. (Compare this speed map with fig. 15(f).)

Reference 25 describes free-free modal testing performed on individual gears with no bearings, spacers, etc., installed. The results are reported in the form of Campbell diagrams. For the input pinions resonances were found at 5500 Hz (pinion shaft) and at 5800/6200 Hz (two-dimensional gear ring at 100-percent speed). Free-free modal testing will detect flexible body modes but not rigid body modes in which the pinion and gear move relative to their supports and to each other. Therefore additional modes may be present. No damping rings were installed on the input pinions (ref. 25) because none of the modes found coincided with the first harmonic of any tooth meshing frequency. The modal testing was not performed with the pinion installed with bearings, etc., in the transmission case. However, reference 14 reports less than a 10-percent increase in modal frequencies between free and installed states.

The sidebands associated with gear meshing frequency measured at VIB 8 (fig. 17) are shown as zoom spectra on a logarithmic amplitude scale with a frequency resolution of 0.78 Hz. The horizontal line at 0 dB indicates the 1.0-g reference level. (Compare the discrete frequency lines of fig. 17 with those of fig. 15(d).) The presence of gear shaft runout would be indicated by strong sidebands, but here the sidebands are at least 20 dB lower than the associated gear mesh frequency. These low levels indicate very little shaft runout in the right input pinion and gear.

The right input pinion produced consistently higher vibration (typically 50 percent higher g-levels) than the identical left input pinion throughout the testing sequence. The cause for this difference is suspected to be transmission error combined with an undamped resonance condition at the right input pinion (see the section Post-Test Inspection). The left input vibration levels (VIB 2 and VIB 9, figs. 13 and 18) were also less torque dependent (figs. 12(a) and (g)) and show much less evidence of resonance.

Of the 11 accelerometers the three on the transmission mounting arms produced similar data, and therefore only one of these (VIB 3) is reported in table III. Another was mounted on the split line between the upper and lower housings to monitor ring gear vibration levels. Its values were consistently low (less than 2 g's rms) and are not further reported.

VIB 7.—The forward accessory pinion (VIB 7, figs. 12(e) and 20(c)) showed a strong 30.9-g component in its spectrum at 2991 Hz. This is the common meshing frequency (at 99 percent speed) of the four pinions that mesh with the main bevel gear (two input pinions and two accessory pinions). In the test transmission the forward accessory pinion operated without load because the transmission was tested with no forward accessory gearbox.

VIB 5/6.—The vibration signals measured on the rotor housing near the output bearing (VIB 5 and VIB 6, figs. 14 and 20(a)) were dominated by planet meshing (i.e., sun/planet and planet/ring) frequencies. The second planet harmonic was relatively prominent in most of these spectra. Planet harmonics were greatly diminished at the low torque operating conditions, especially at the 99-percent speed and 11-percent torque of VIB 5 (fig. 14(f)). The torque dependence of the vibration level shows clearly in figures 12(c) and (d) (VIB 5 and VIB 6). Torque dependence suggests that tooth deflection is a major contributor to transmission error for the planetary gears. Houser (ref. 30) discusses the effect of transmission error on the compliance (deflection) of gear teeth. The first two planet mesh harmonics of VIB 6 are shown at expanded scale in figure 20(b) to display the sideband structure. Sidebands were distributed at the planet passing frequency (19 Hz) about the planet meshing harmonics. The amplitude of the sidebands was not more than 20 percent of the associated harmonic frequency. This suggests that the planet gears had little runout. The sidebands are distributed in a nonsymmetrical pattern about the tooth meshing frequency. The distortion effects of ring gear deflection acting at planet passing would produce a symmetrical pattern of tooth positioning errors (frequency modulation) plus a cyclic variation in the depth of gear tooth engagement (amplitude modulation). The two types of modulation acting together produce the typical nonsymmetrical pattern (ref. 15).

Additional sources of asymmetry include multiple mesh contact (due to the presence of several planets) and the smoothing effect of multiple tooth contact as vibration energy is transmitted through the gear mesh into the surrounding structure. A mathematical treatment of gear-transmission-error (in the frequency domain) mesh transfer functions appears in reference 19. For a discussion on planet passing vibration, see reference 32.

Vibration frequencies attributable to rolling-element bearings have not been identified. Minor bearing faults are not apparent in transmission gearbox spectra because of the overall dominance of gear meshing signals. Bearing faults can be difficult to detect unless transducers are mounted directly on bearing races (refs. 34 and 35).

Post-Test Inspection

The transmission was inspected after 50 hr of testing. The transmission oil particulate analysis revealed no significant increase in contaminant level. Oil system component surface integrities were acceptable. The general overall appearance of the gears and bearings was indicative of moderate to full loading. Light wearing of the black oxide coating on the load surfaces of the gears revealed the contact pattern. No spalling was observed. In figures 21 to 25 the adjacent tooth was painted white to highlight the gear tooth contact area by light reflectance.

The right input spiral-bevel pinion gear (fig. 21) had poor tooth contact with its mating bevel gear. The load-side contact

pattern (footprint) was positioned approximately normally at the gear tooth heel, but the contact area dropped below the pitch diameter and to near line contact at the toe. The poor contact pattern is suspected to be a result of angular misalignment. Poor tooth contact between pinion and gear is expected to cause tooth positioning errors (the mean component of transmission error) as the gear tooth rolls through the mesh. Tooth positioning errors excite harmonics of the tooth mesh frequency, and this combined with the resonance band observed (4500 to 6000 Hz, see VIB 8) is indicative of the cause of the high vibration levels measured at the right input pinion. The main bevel gear (fig. 22) as well as the left input pinion gear showed acceptable contact patterns. On the planetary stage (fig. 23) the addendum portion of the sun gear showed scuffing under strong, low-incident side lighting, indicating tip interference. The mottled appearance of the addendum also shows wear degradation of the surface, indicating a need for more tip relief. This degradation is consistent with the noted vibration harmonic sideband structure of VIB 6. One of the four planet gears (fig. 24) displayed light tooth addendum (tip) scuffing and a well-positioned contact area footprint. The footprint of the ring gear (fig. 25) displayed only loading effects.

The bearings in the main power flow path (roller, tapered roller, and ball) were visually inspected. There were no significant flaws that could contribute to the operational results reported herein.

Facility

The NASA Lewis 2240-kW (3000-hp) transmission test facility was initially operated at power levels to 2600 kW (3500 hp) so as to qualify all systems for testing advanced helicopter transmissions. The facility can be modified to allow testing of transmissions similar in power level but with different input and tail shaft configurations. The input configurations can range from opposite facing (lateral) to two parallel fore-aft facing. The input speed range is 7000 to 22 000 rpm with facility gearbox modifications (fig. 1).

The remote control room contains minicomputer and mainframe data acquisition and reduction capabilities. During full-scale performance testing of advanced helicopter transmissions the state-of-the-art instrumentation can also obtain data on the condition of internal components and subsystems. The data will allow analytical computer code verifications relating to increasing both the efficiency and the MTBUR and P/W performance indices of helicopter transmissions.

Summary of Results

A helicopter transmission that was considered for the Army's Utility Tactical Transport Attack System (UTTAS) was tested in the NASA Lewis 2240-kW (3000-hp) test facility to obtain baseline efficiency and vibration data for use as a data base for evaluating similar-power-class transmissions.

The following results were obtained:

1. The mechanical efficiency of the YUH-61A helicopter transmission, when tested at its rated power level of 2080 kW (2792 hp), was 98.7 percent.
2. At 113 percent of nominal rated torque and 100 percent of nominal rated speed, most of the vibration meter acceleration levels ranged from 3 to 25 g's rms.
3. For the right input the vibration meter level was 39 g's rms at 113 percent of nominal rated power, 56 percent higher than for the left input. Teardown inspection revealed poor tooth contact of the right spiral-bevel pinion gear.
4. The highest vibration level, 52 g's rms, was measured at the aft accessory gearbox.
5. The facility was operated and qualified for testing to 2600 kW (3500 hp).

National Aeronautics and Space Administration
Lewis Research Center
Cleveland, Ohio 44135, December 4, 1985

References

1. Shipley, E.E.: Loaded Gears in Action. Gear Handbook, D.W. Dudley, ed., McGraw Hill, 1962, pp. 14-1 to 14-60.
2. Martin, K.F.: A Review of Friction Predictions in Gear Teeth. Wear, vol. 49, no. 2, Aug. 1978, pp. 201-238.
3. Martin, K.F.: The Efficiency of Involute Spur Gears. J. Mech. Des., vol. 103, no. 1., Jan. 1981, pp. 160-169.
4. Anderson, N.E.; and Loewenthal, S.H.: Effect of Geometry and Operating Conditions on Spur Gear System Power Loss. J. Mech. Des., vol. 103, no. 1, Jan. 1981, pp. 151-159.
5. Anderson, N.E.; and Loewenthal, S.H.: Spur Gear System Efficiency at Part and Full Load. NASA TP-1662, 1980.
6. Townsend, D.P.; and Akin, L.S.: Study of Lubricant Jet Flow Phenomena in Spur Gears—Out of Mesh Condition. J. Mech. Des., vol. 100, no. 1, Jan. 1978, pp. 61-68.
7. Townsend, D.P.; and Akin, L.S.: Analytical and Experimental Spur Gear Tooth Temperature as Affected by Operating Variables. J. Mech. Des., vol. 103, no. 1, Jan. 1981, pp. 219-226.
8. Akin, L.S.; and Townsend, D.P.: Cooling of Spur Gears with Oil Jet Directed into the Engaging Side of Mesh at Pitch Point. Proceedings of the JSME International Symposium on Gearing and Power Transmissions, Tokyo, 1981, Vol. 1, Paper B4, pp. 261-274.
9. Murphy, W.R.: The Effect of Lubricant Traction on Wormgear Efficiency. AGMA Paper, Oct. 1981, p. 254.33.
10. Townsend, D.P.; Allen, C.W.; and Zaretsky, E.V.: Study of Ball Bearing Torque Under Elastohydrodynamic Lubrication. J. Lubr. Technol., vol. 96, no. 4, Oct. 1974, pp. 561-571.
11. Weden, G.J.; and Coy, J.J.: Summary of Drive Train Component Technology in Helicopters. NASA TM-83726, 1984.
12. Mitchell, A.M.; and Coy, J.J.: Lubrication Effects on Efficiency of a Helicopter Transmission. NASA TM-82857, 1982.
13. Coy, J.J.; Mitchell, A.M.; and Hamrock, B.J.: Transmission Efficiency Measurements and Correlations with Physical Characteristics of the Lubricant. NASA TM-83740, 1984.
14. Drago, R.J.; and Brown, F.W.: The Analytical and Experimental Evaluation of Resonant Response in High-Speed, Lightweight, Lightly Loaded Gearing. ASME Paper 80-C2-DET-22, Aug. 1980.

15. Dale, A.K.: Gear Noise and the Sideband Phenomenon, ASME Paper 84 DET-174, Oct. 1984.
16. Smith, J.D.: Gears and Their Vibration. Marcel Dekker, Inc., New York, 1983.
17. Trouve and Chabassieu: Experimental Model Analysis. Assoc. Aeronautique & Astronautique de France, Paper 7.1. Presented at the 8th European Rotorcraft Forum, Aix-En-Provence, France, Sept. 1982.
18. Randall, R.B.: Cepstrum Analysis and Gearbox Fault Diagnosis. Edition 2. Bruel and Kjaer Application Note 233-80, 1980.
19. Mark, W.D.: Gear Noise Excitation. Engine Noise: Excitation, Vibration, and Radiation, R. Hickling and M.M. Kamal, eds., Plenum Publishing Corp., 1982.
20. Zaretsky, E.V.; Coy, J.J.; and Townsend, D.P.: NASA Transmission Research and Its Probable Effects on Helicopter Transmission Design. NASA TM-83389, 1983.
21. Zaretsky, E.V.: NASA Helicopter Transmission Systems Technology Program. Proceedings of the Advanced Power Transmission Technology Symposium, NASA CP-2210, 1982, pp. 15-33.
22. Mancini, Z.R.: Helicopter Gearbox Testing. Helicopter Fatigue Life Assessment Conference. AGARD CP-297, 1981, pp. 11-1 to 11-10.
23. Baker, A.H.: Fatigue Testing of Helicopter Gearboxes. Helicopter Fatigue Life Assessment Conference. AGARD CP-297, 1981, pp. 12-1 to 12-23.
24. Jones, H.D.: Ground Test Vehicle Testing. U.S. Army Aviation Research / Development Command, 35th Annual Forum of the American Helicopter Society, May 1979.
25. Model YUH-61A Helicopter Drive System: Main Transmission Endurance and Reliability Qualification Test. Boeing Vertol Report T179-10057-1 (Final Report). Boeing Vertol Co., 1976.
26. Standard Handbook for Mechanical Engineers. T. Baumeister and L.S. Marks, eds., 7th Edition, 1967.
27. Kleckner, R.J.; Dyba, G.J.; and Ragen, M.A.: SPHERBEAN User's Manual. SKF AT-81D007. Feb. 1982, Appendix B, pp. 106-113.
28. Senholzi, P.B.: Oil Analysis. NAEC 92-153, Aug. 1982.
29. Present, D.L.; Newman, F.M.; Tyler, J.C.; and Cuellar, J.P.: Advanced Chemical Characterization and Physical Properties of Eleven Lubricants. NASA CR-168187, 1983.
30. Houser, D.R.: Gear Noise Sources and Their Prediction Using Mathematical Models. Original Equipment Manufacturers (OEM) Conference, Philadelphia, PA, Sept. 11, 1985.
31. Gu, A.L.; and Badgley, R.H.: Prediction of Vibration Sidebands in Gear Meshes," ASME Paper 74-DET-95, Oct. 1974.
32. Gu, A.L.; Badgley, R.H.; and Chiang, T.: Planet-Pass-Induced Vibration in Planetary Reduction Gears. ASME Paper 74-DET-93, Oct. 1974.
33. Houser, D.R.: Basis for Spectral Analysis. Fifth Turbomechanics Seminar: Spectral Analysis in Machinery Health Monitoring, Paper 1, Sept. 1978.
34. Houser, D.R.; and Drosjack, M.J.: Vibration Signal Analysis Techniques. USAAMRDL TR-73-101, 1973.
35. Volker, E.; and Martin, H.R.: Early Detection of Damage in Rolling Bearings. ISA Trans., vol. 23, no. 3, 1984, pp. 27-32.

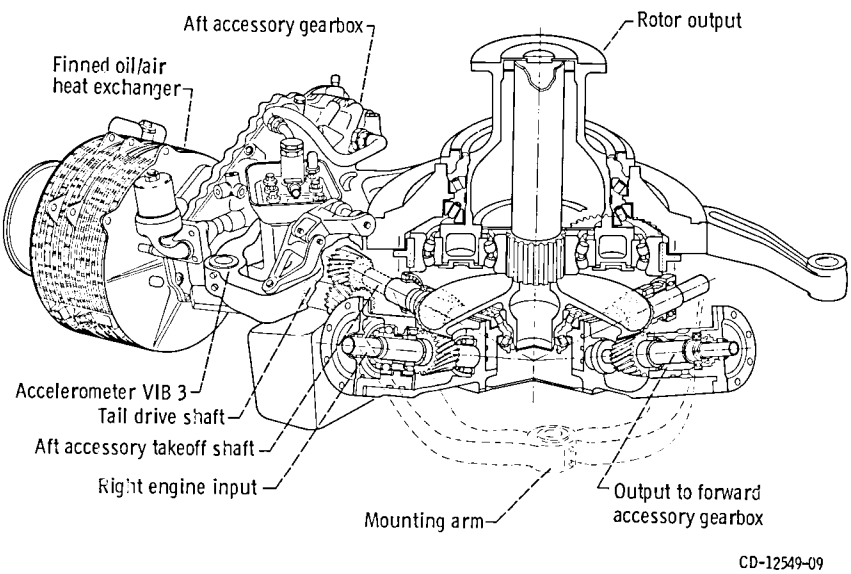

Figure 1.—YUH-61A transmission.

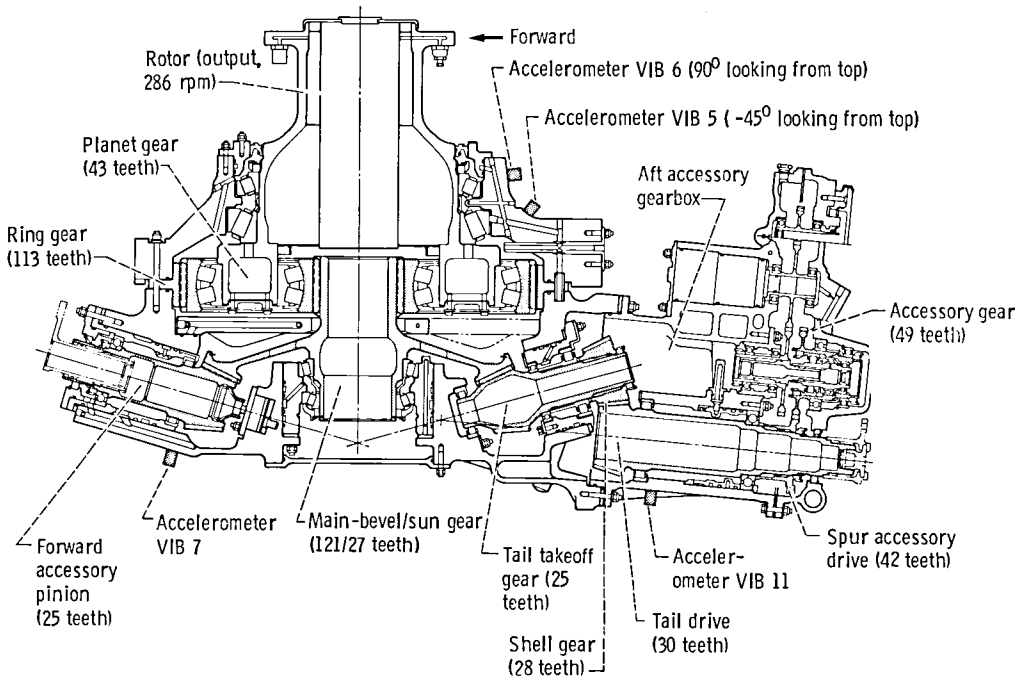

Figure 2.—Side view of YUH-61A transmission.

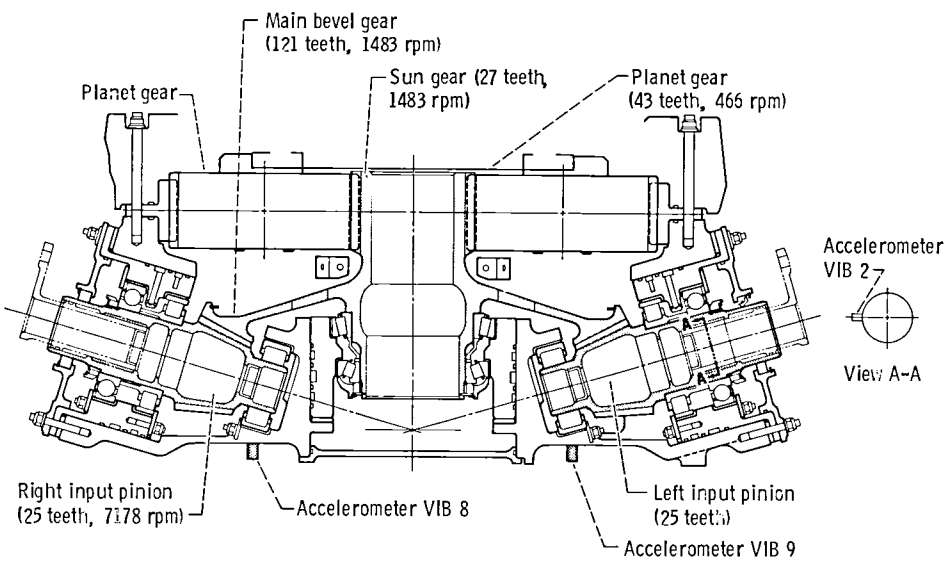

Figure 3.—Aft view of YUH-61A transmission.

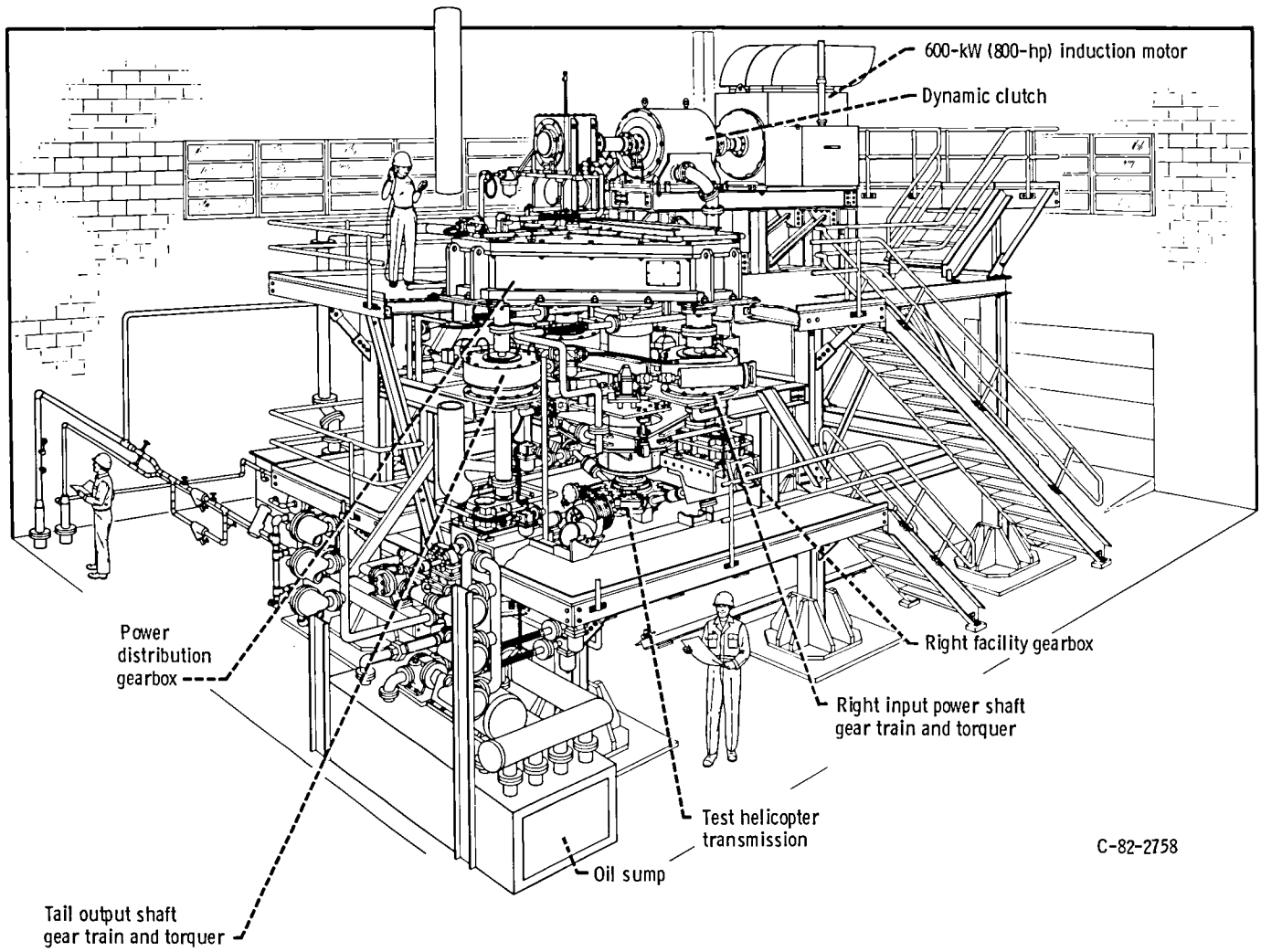

Figure 4.—NASA Lewis 2240-kW (3000-hp) transmission facility.

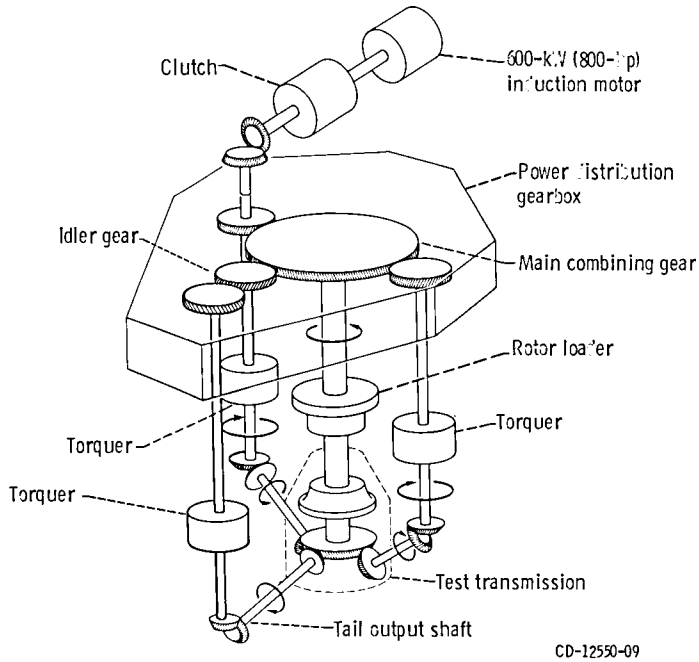

Figure 5.—Schematic of helicopter transmission test stand.

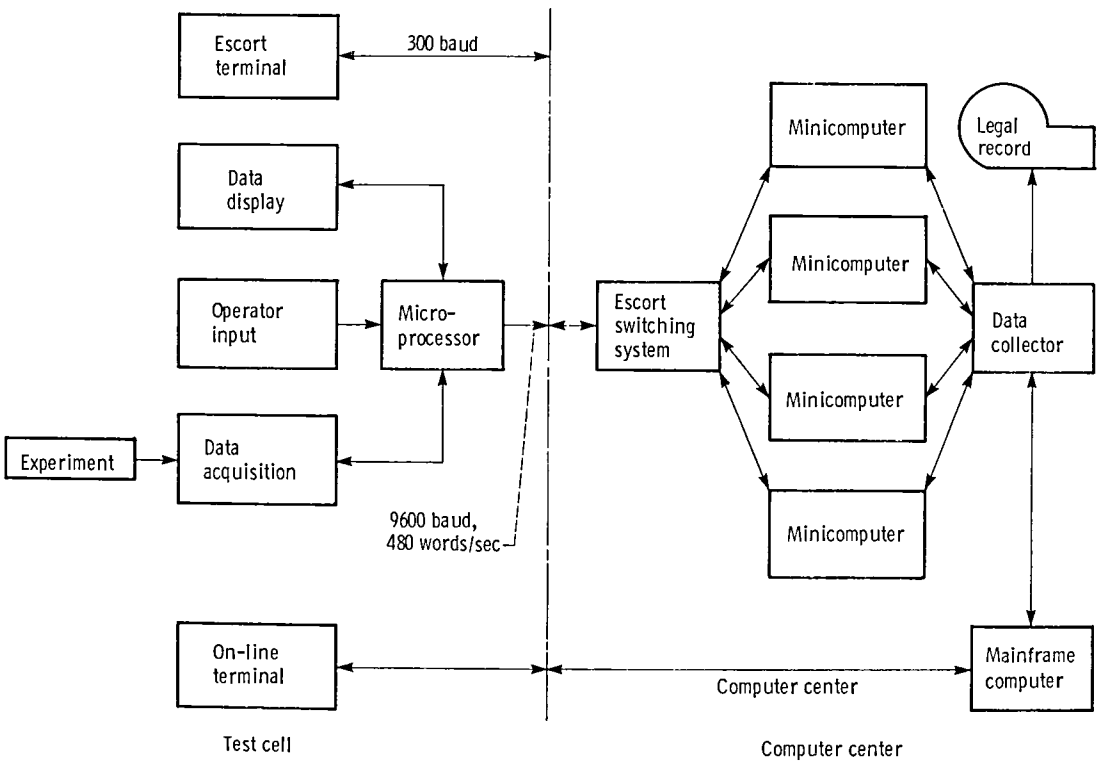

Figure 6.—Escort II data acquisition system.

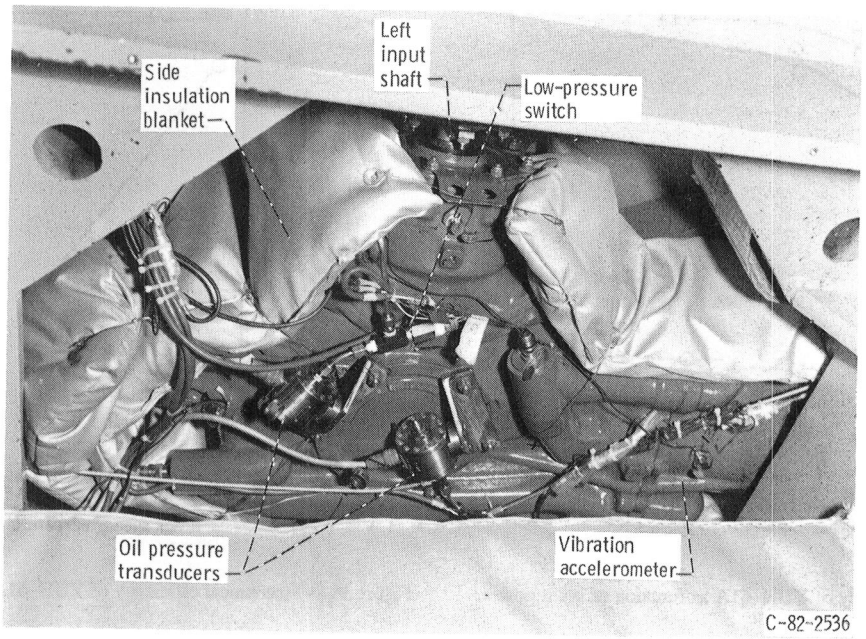

Figure 7.—Underside of YUH-61A transmission showing insulated side blanket and instrumentation.

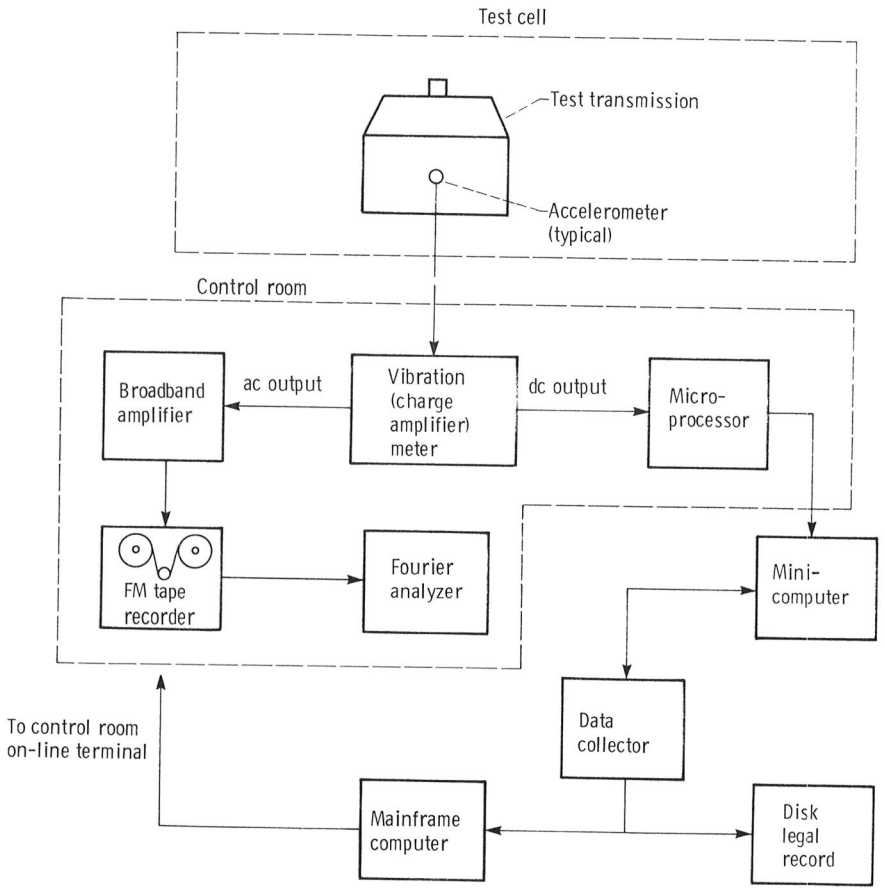

Figure 8.—Vibration measurement system.

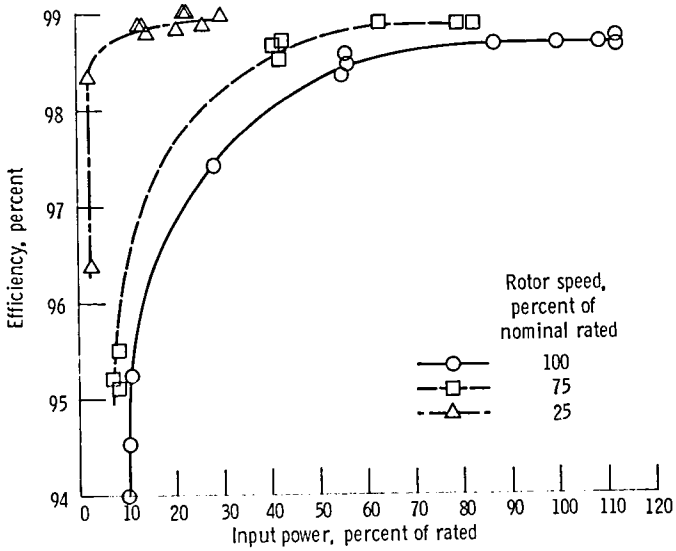

Figure 9.—Mechanical efficiency of YUH-61A as function of input power.

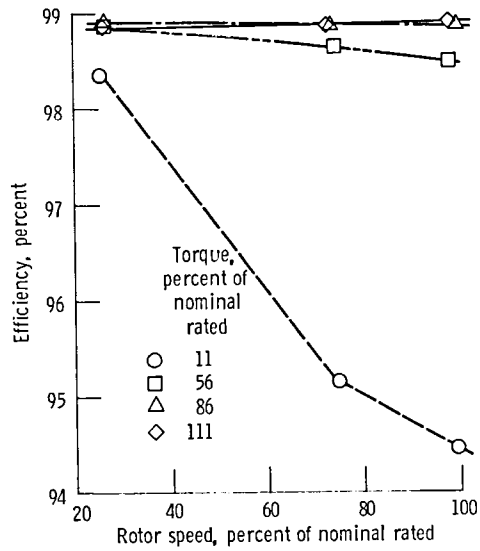

Figure 11.—Mechanical efficiency of YUH-61A as function of rotor speed.

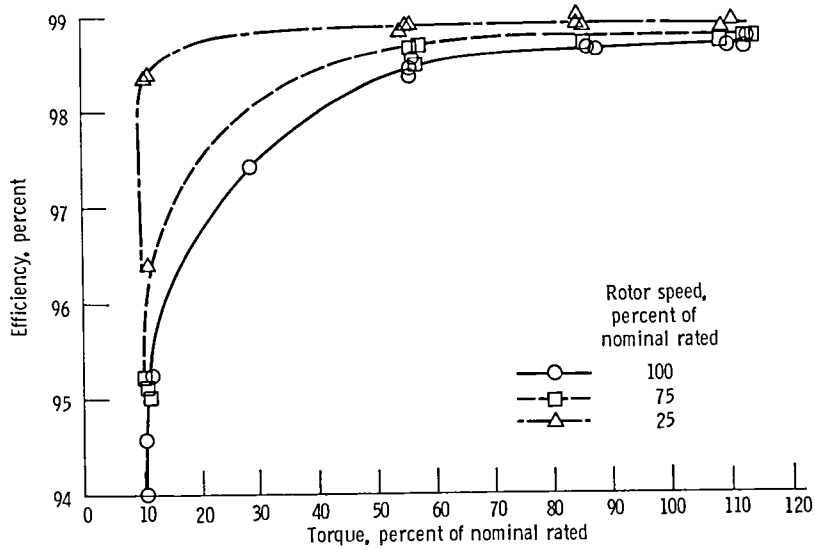

Figure 10.—Mechanical efficiency of YUH-61A as function of input torque.

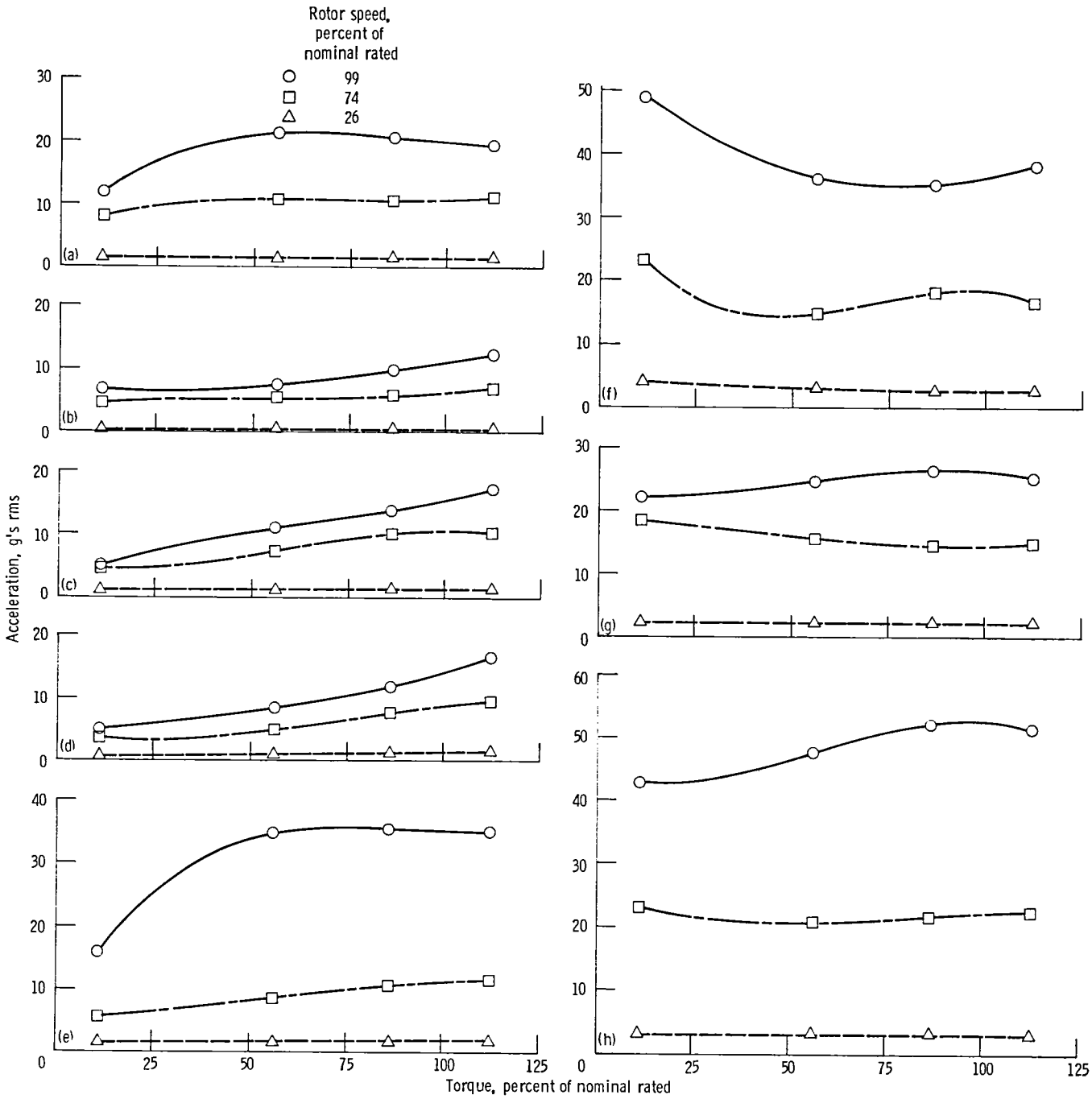

(a) VIB 2, left input, horizontal.
(b) VIB 3, right rear mounting arm.
(c) VIB 5, rotor housing, −45°.
(d) VIB 6, rotor housing, horizontal.
(e) VIB 7, forward accessory pinion.
(f) VIB 8, right input pinion.
(g) VIB 9, left input pinion.
(h) VIB 11, aft accessory drive case.

Figure 12.—Vibration amplitude as function of rotor speed and torque (see figs. 1 to 3 for accelerometer locations).

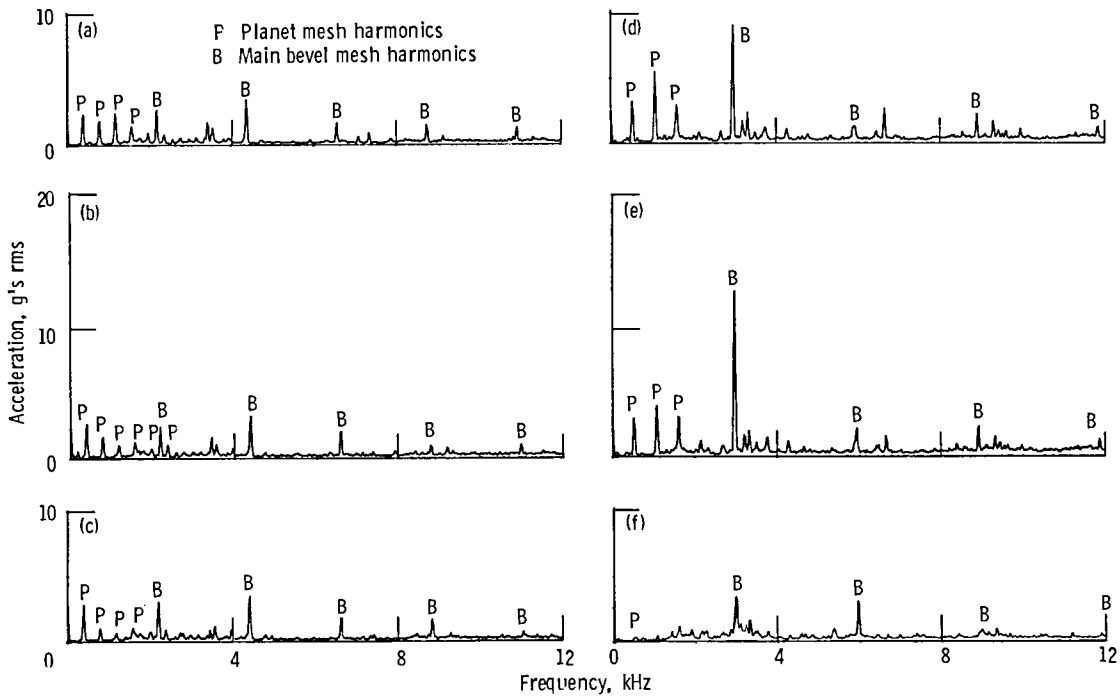

(a) Rotor speed, 73 percent nominal rated; torque, 112 percent of nominal rated.
(b) Rotor speed, 73 percent nominal rated; torque, 88 percent of nominal rated.
(c) Rotor speed, 76 percent nominal rated; torque, 58 percent of nominal rated.
(d) Rotor speed, 99 percent nominal rated; torque, 113 percent of nominal rated.
(e) Rotor speed, 100 percent nominal rated; torque, 88 percent of nominal rated.
(f) Rotor speed, 99 percent nominal rated; torque, 11 percent of nominal rated.

Figure 13.—Vibration spectra for VIB 2 (left input horizontal).

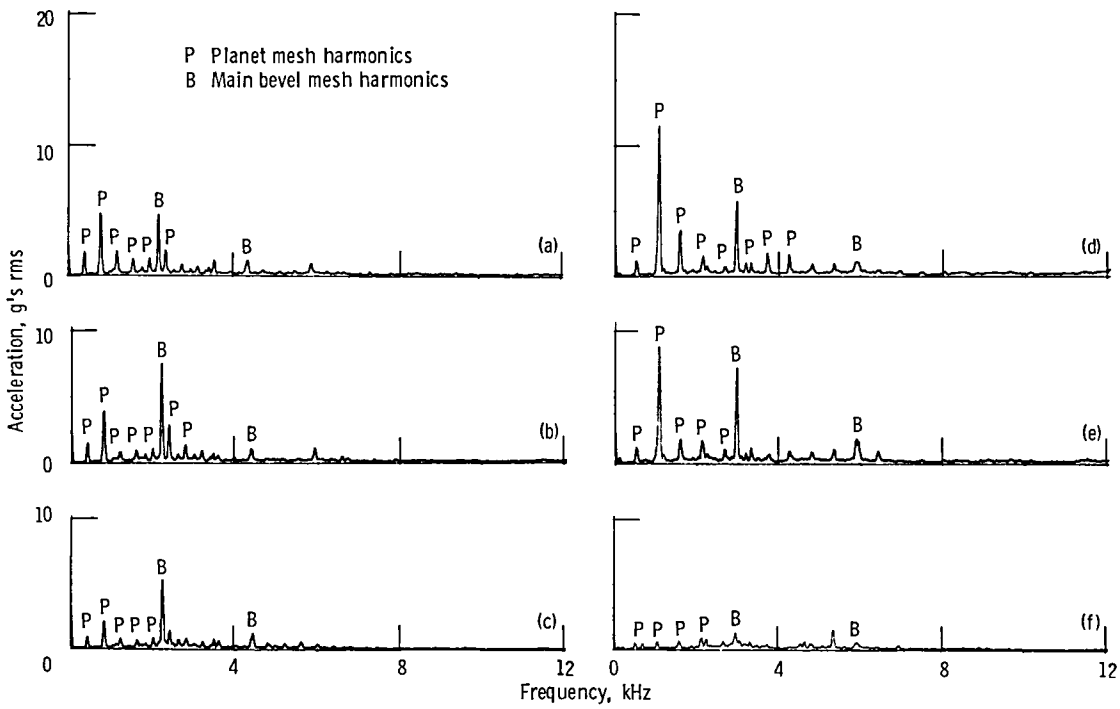

(a) Rotor speed, 73 percent nominal rated; torque, 112 percent of nominal rated.
(b) Rotor speed, 73 percent nominal rated; torque, 88 percent of nominal rated.
(c) Rotor speed, 76 percent nominal rated; torque, 58 percent of nominal rated.
(d) Rotor speed, 99 percent nominal rated; torque, 113 percent of nominal rated.
(e) Rotor speed, 100 percent nominal rated; torque, 88 percent of nominal rated.
(f) Rotor speed, 99 percent nominal rated; torque, 11 percent of nominal rated.

Figure 14.—Vibration spectra for VIB 5 (rotor housing, 45°).

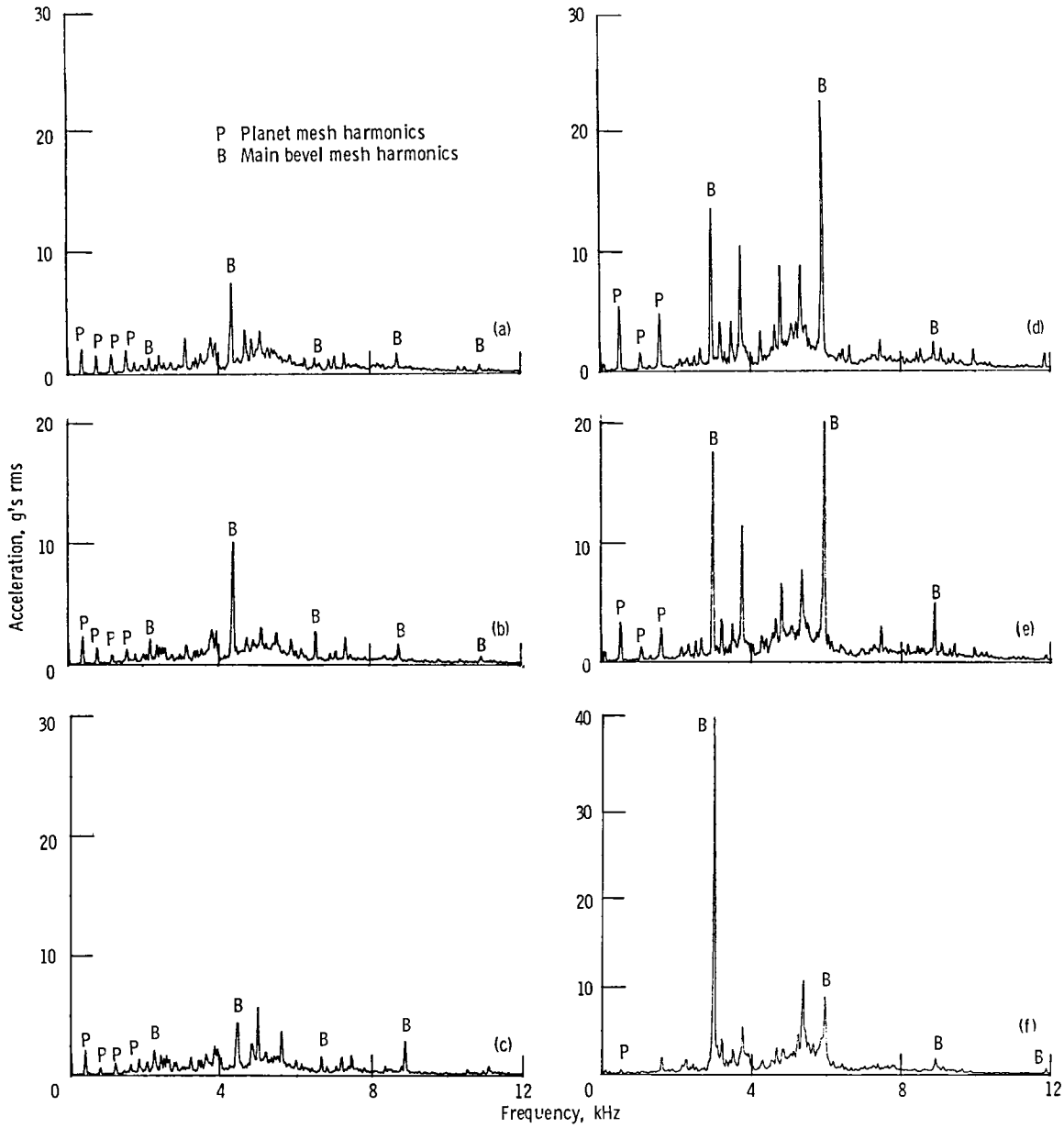

(a) Rotor speed, 73 percent nominal rated; torque, 112 percent of nominal rated.
(b) Rotor speed, 73 percent nominal rated; torque, 88 percent of nominal rated.
(c) Rotor speed, 76 percent nominal rated; torque, 58 percent of nominal rated.
(d) Rotor speed, 99 percent nominal rated; torque, 113 percent of nominal rated.
(e) Rotor speed, 100 percent nominal rated; torque, 88 percent of nominal rated.
(f) Rotor speed, 99 percent nominal rated; torque, 11 percent of nominal rated.

Figure 15.—Vibration spectra for VIB 8 (right input pinion).

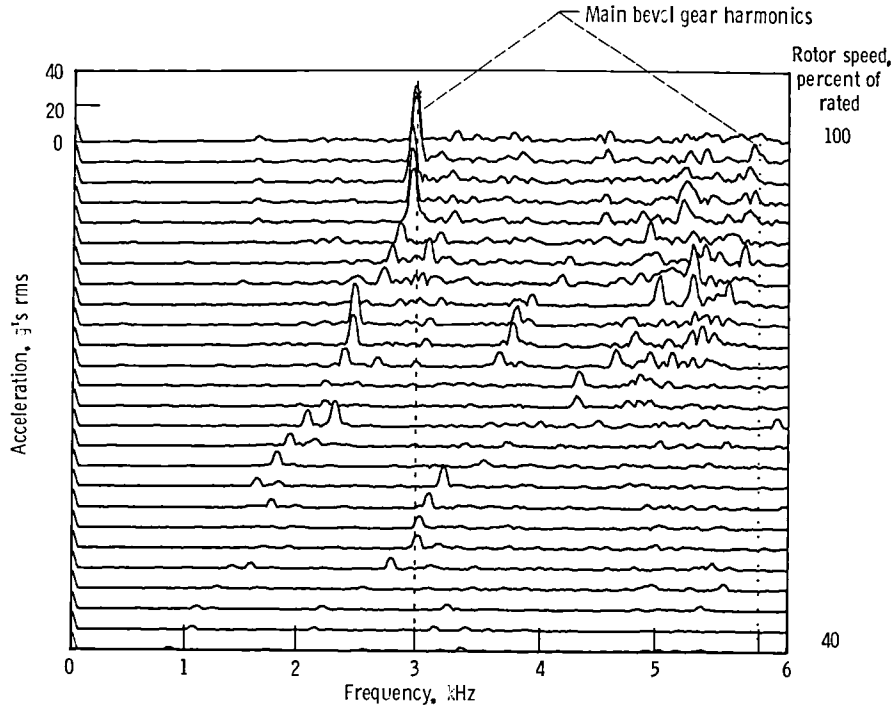

Figure 16.—Speed map for VIB 8 (right input pinion). Torque, 11 percent of rated.

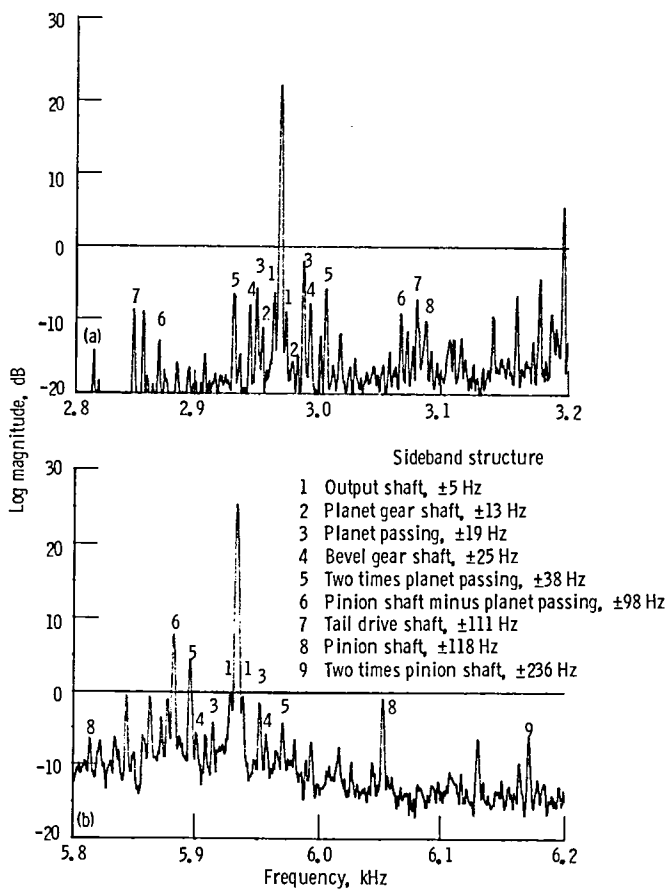

(a) First harmonic (2963 Hz).
(b) Second harmonic, 5926 Hz.

Figure 17.—Zoom spectra showing sideband structure for VIB 8 (right input pinion). Rotor speed, 99 percent of rated; torque, 113 percent of rated.

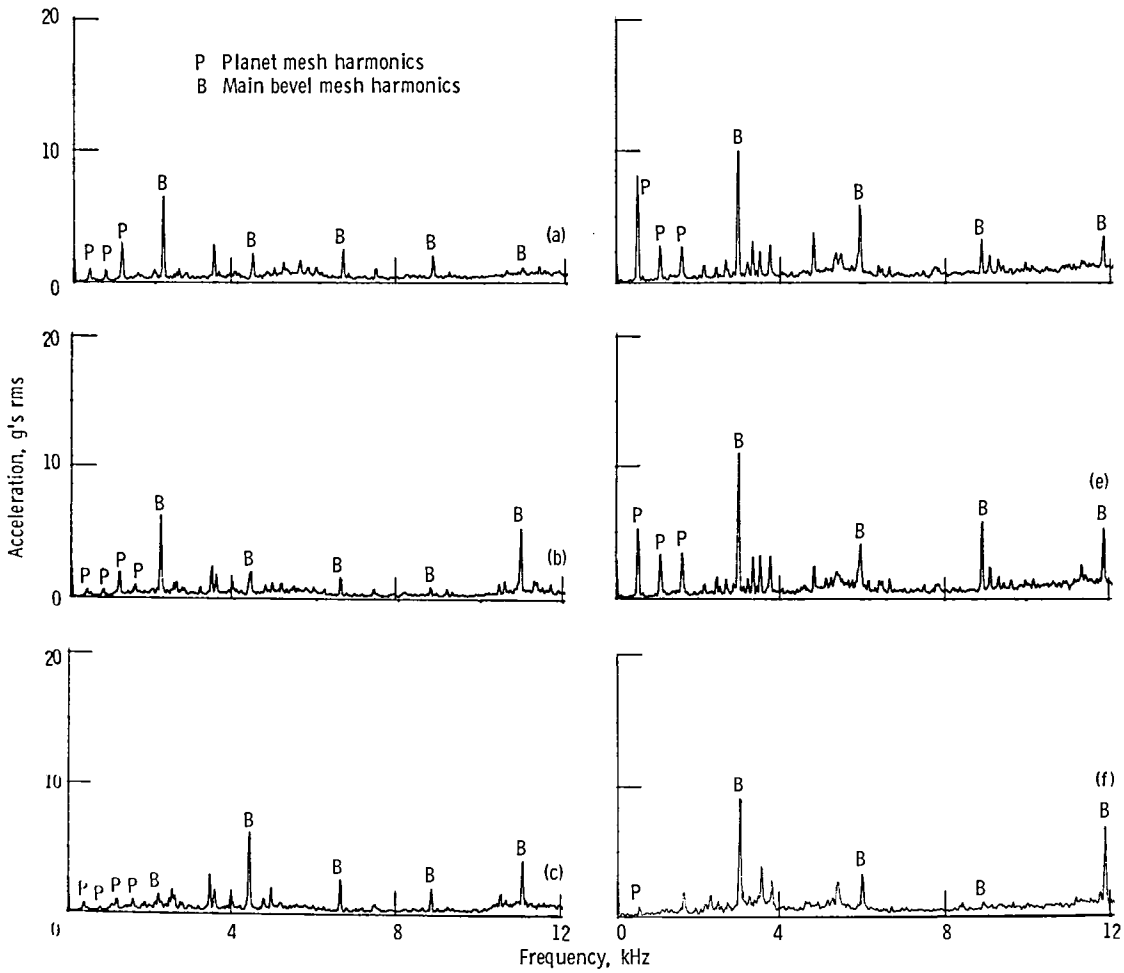

(a) Rotor speed, 73 percent nominal rated; torque, 112 percent of nominal rated.
(b) Rotor speed, 73 percent nominal rated; torque, 88 percent of nominal rated.
(c) Rotor speed, 76 percent nominal rated; torque, 58 percent of nominal rated.
(d) Rotor speed, 99 percent nominal rated; torque, 113 percent of nominal rated.
(e) Rotor speed, 100 percent nominal rated; torque, 88 percent of nominal rated.
(f) Rotor speed, 99 percent nominal rated; torque, 11 percent of nominal rated.

Figure 18.—Vibration spectra for VIB 9 (left input pinion).

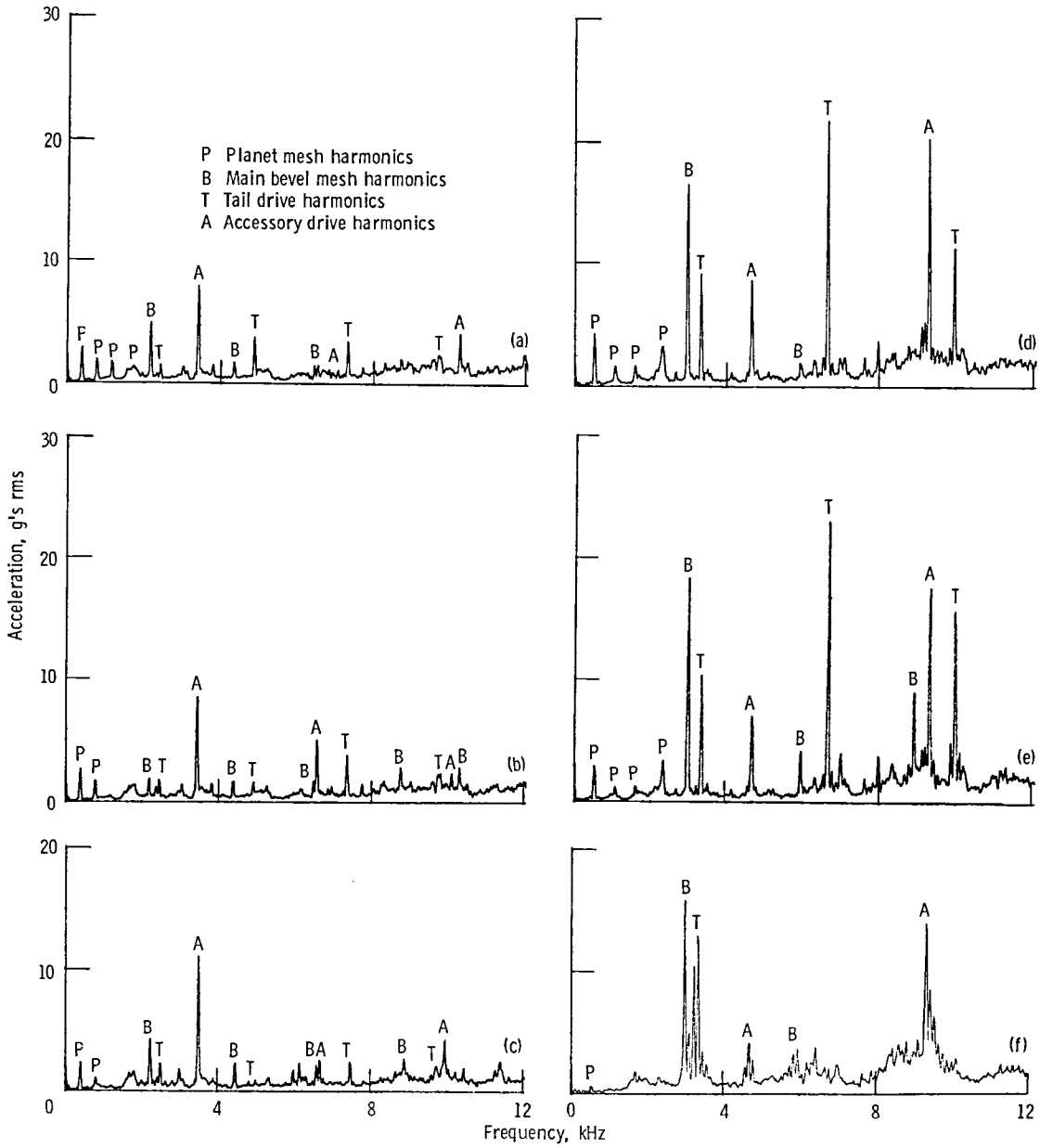

(a) Rotor speed, 73 percent nominal rated; torque, 112 percent of nominal rated.
(b) Rotor speed, 73 percent nominal rated; torque, 88 percent of nominal rated.
(c) Rotor speed, 76 percent nominal rated; torque, 58 percent of nominal rated.
(d) Rotor speed, 99 percent nominal rated; torque, 113 percent of nominal rated.
(e) Rotor speed, 100 percent nominal rated; torque, 88 percent of nominal rated.
(f) Rotor speed, 99 percent nominal rated; torque, 11 percent of nominal rated.

Figure 19.—Vibration spectra for VIB 11 (aft accessory drive case).

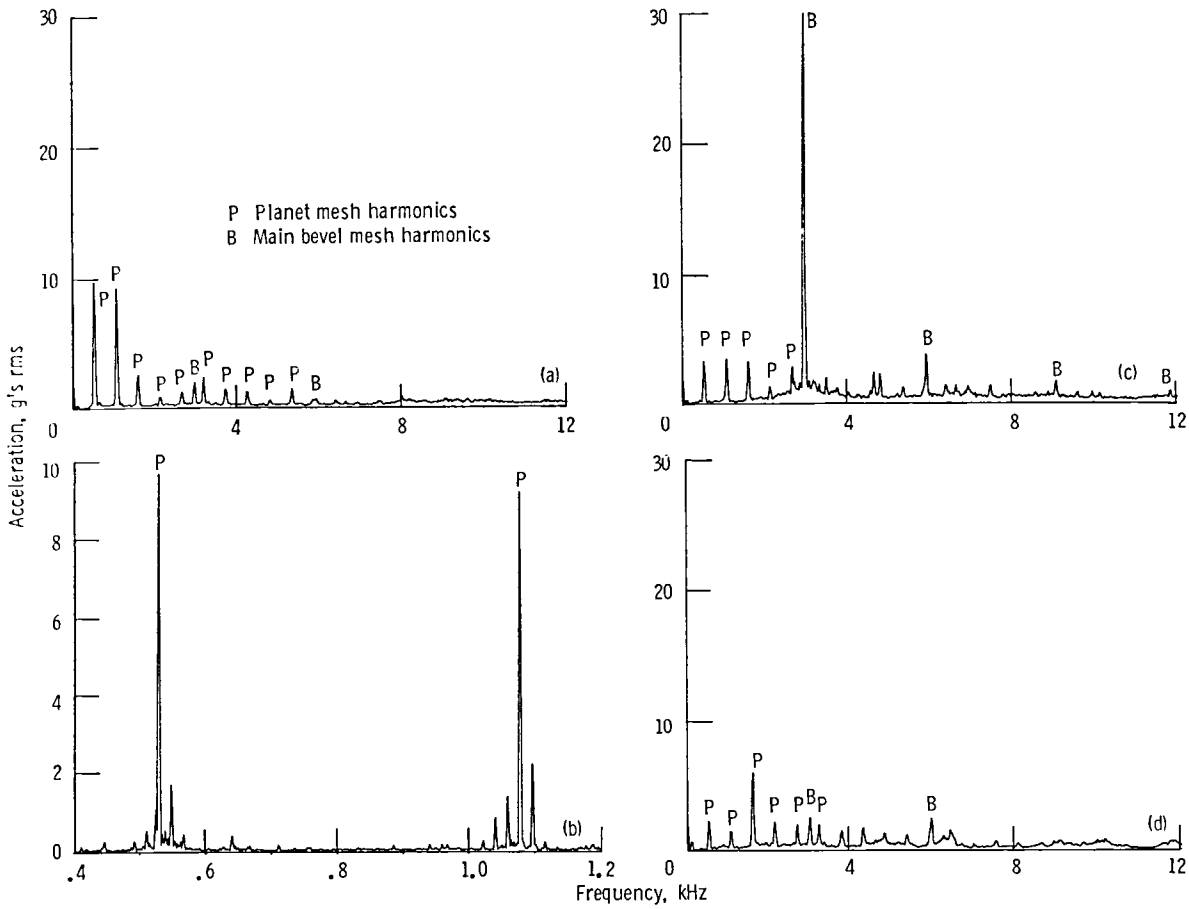

(a) VIB 6, rotor housing, horizontal.
(b) First two planetary harmonics from (a).
(c) VIB 7, forward accessory pinion.
(d) VIB 3 right rear mounting arm.

Figure 20.—Vibration spectra for various locations. Rotor speed, 99 percent of rated; torque, 113 percent of rated.

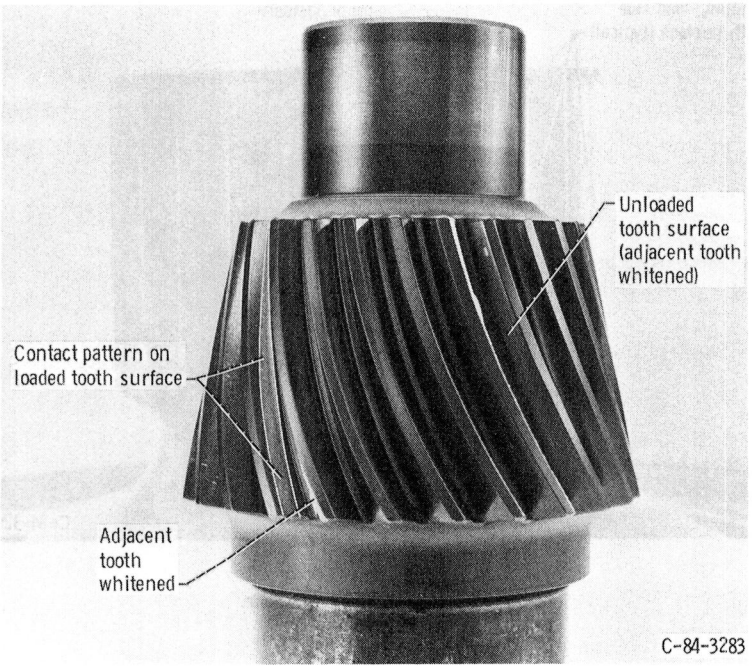

Figure 21.—Right input spiral-bevel pinion gear.

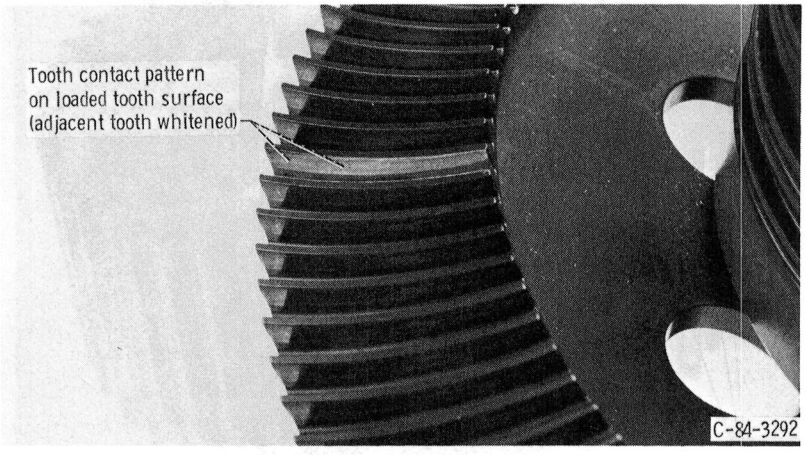

Figure 22.—Main bevel gear.

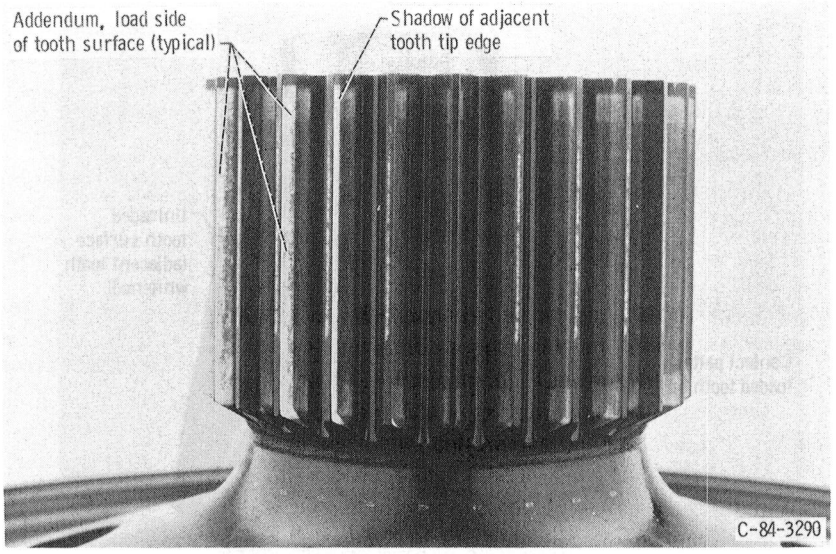

Figure 23.—Main-bevel sun gear.

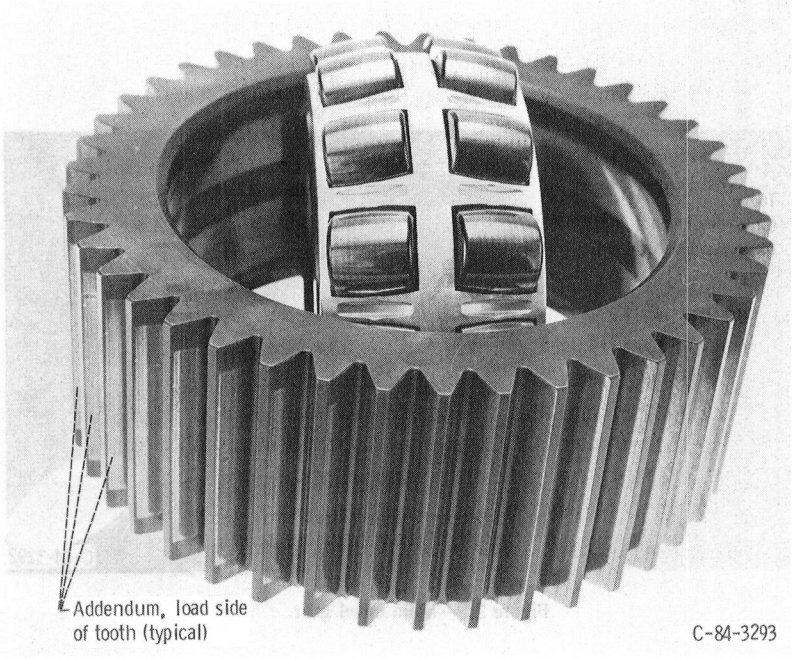

Figure 24.—Planet gear and bearing.

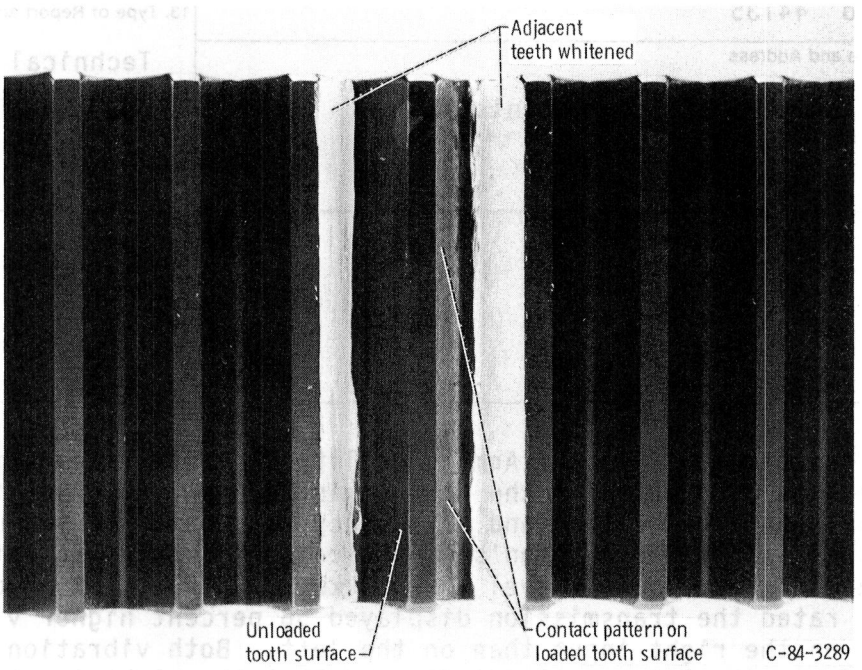

Figure 25.—Ring gear.

1. Report No.	2. Government Accession No.	3. Recipient's Catalog No.
NASA TP-2538		

4. Title and Subtitle	5. Report Date
Testing of YUH-61A Helicopter Transmission in NASA Lewis 2240-kW (3000-hp) Facility	March 1986
	6. Performing Organization Code: 505-62-51

7. Author(s)	8. Performing Organization Report No.
Andrew M. Mitchell, Fred B. Oswald, and Fredrick T. Schuller	E-2801
	10. Work Unit No.

9. Performing Organization Name and Address	11. Contract or Grant No.
National Aeronautics and Space Administration Lewis Research Center Cleveland, Ohio 44135	
	13. Type of Report and Period Covered: Technical Paper

12. Sponsoring Agency Name and Address	14. Sponsoring Agency Code
National Aeronautics and Space Administration Washington, D.C. 20546	

15. Supplementary Notes

16. Abstract

A helicopter transmission from the Army's Utility Tactical Transport Attack System (UTTAS) competition was tested in the NASA Lewis 2240-kW (3000-hp) test facility. The results will form a vibration and efficiency data base for evaluating similar-class helicopters. The transmission's mechanical efficiency was determined to be 98.7 percent at its rated power level of 2080 kW (2792 hp). At power levels to 113 percent of rated the transmission displayed 56 percent higher vibration acceleration levels on the right input than on the left. Both vibration signature analysis and final visual inspection indicated that the right input spiral-bevel gear had poor contact patterns. Other vibration levels are reported. The test facility was operated and qualified for testing to 2600 kW (3500 hp).

17. Key Words (Suggested by Author(s))	18. Distribution Statement
Helicopter transmission Vibration Efficiency	Unclassified - unlimited STAR Category 37

19. Security Classif. (of this report)	20. Security Classif. (of this page)	21. No. of pages	22. Price
Unclassified	Unclassified	26	A03

For sale by the National Technical Information Service, Springfield, Virginia 22161

NASA-Langley, 1986